Design of Creep–Resistant Steel Welds

H. K. D. H. Bhadeshia

University of Cambridge
Department of Materials Science and Metallurgy
Pembroke Street, Cambridge CB2 3QZ, U.K.

Published in: *Trends in Welding Research,* eds. S. A. David, T. DebRoy, J. A. Johnson, H. B. Smartt and J. M. Vitek, ASM International, Ohio, 1999, 795–804.

Abstract

Creep resistant welding alloys must be reliable over long periods of time in severe environments. Their microstructures have to be very stable, both in the wrought and in the welded states. This paper deals with quantitative methods for the design of steel weld metals for elevated temperature applications. A methodology is described for the calculation of complex precipitation reactions over periods extending many tens of years. However, microstructure alone is not enough in the design of alloys. The calculation of complex mechanical properties (such as creep rupture stress) based on a remarkable semi–empirical method in the second part of this review.

Introduction

Typical operating parameters for steels used in the manufacture of power plant are compared against corresponding parameters for nickel alloys in aeroengines, in Table 1. In both cases, the service conditions are severe. But this is especially so for steels where the service life is many decades. The degree of reliability demanded of heat resistant steels is therefore extraordinary, and must represent one of the highest achievements of technology. By contrast, computers (which are frequently identified with advanced technology) seldom last for more than two years and are usually obsolete when installed!

With the benefit of this knowledge, it should not be surprising that the number of variables involved in the design of creep–resistant steels is very large – in fact, we shall show later that there are at least thirty variables which need to be controlled in any experiment or calculation of creep properties. These variables determine the *microstructure* and *mechanical properties*, the key components of any design process.

.

Property	Aeroengine	Power Plant
Temperature	$> 1000\,^{\circ}$C	540-750 $^{\circ}$C
Pressure	$\simeq 3$ bar	160–370 bar
Design life	10^4 h	2.5×10^5 h
$\sigma_{100{,}000\ h}$	10 MPa	100 MPa
Coating	Yes	No
Forced cooling	Yes	No
Single crystal	Yes	No

Table 1: Service conditions for a component in the hot part of an aeroengine and one in the hottest part of a power plant. The lower limits for the power plant component are representative of current technology. The stress is a 100,000 h creep rupture strength.

The variables can ideally be taken into account using what scientists like to call "physical models", *i.e.* theories which explain a large class of observations, which contain few arbitrary elements and which make verifiable predictions. The first part of this paper deals with such physical models in the prediction of microstructure.

There is no adequate theory to deal with the second task, which is the estimation of creep rupture strength as a function of the steel composition and heat treatment. Difficult problems like this, where the general concepts might be understood but which are not as yet amenable to fundamental treatment, are common in metallurgy. To form a complete story it is necessary in such circumstances to resort to learned empiricism. The second part of this paper deals with a semi–empirical method implemented to achieve useful results. The combination of physical and empirical models can then be used to attempt the design of welding alloys!

Before proceeding to a description of models, it is worth pointing out that there is very little distinction made here between steel plate and weld metal. This apparent anomaly is justified towards the end of the paper.

The Microstructure

There is a large range of heat–resistant steels and welding alloys (Table 2). The ones with the lowest solute concentrations might contain substantial quantities of allotriomorphic ferrite and some pearlite, but the vast majority have bainitic or martensitic microstructures in the normalised condition. After normalising the steels are severely tempered to produce a "stable" microstructure consisting of a variety of alloy carbides in a ferritic matrix. The task is therefore to

model the evolution of precipitation and dissolution reactions.

Designation	C	Si	Mn	Ni	Mo	Cr	V
1Cr$\frac{1}{2}$Mo	0.15	0.25	0.50	–	0.6	0.95	
$\frac{1}{4}$CrMoV	0.15	0.25	0.50	0.05	0.50	0.30	0.25
$\frac{1}{2}$Cr$\frac{1}{2}$Mo$\frac{1}{4}$V	0.12	0.25	0.50	–	0.6	0.45	0.25
1CrMoV	0.25	0.25	0.75	0.70	1.00	1.10	0.35
2$\frac{1}{4}$Cr1Mo	0.15	0.25	0.50	0.10	1.00	2.30	0.00
Mod. 2$\frac{1}{4}$Cr1Mo	0.1	0.05	0.5	0.16	1.00	2.30	0.25
						Ti=0.03	B=0.0024
3.0Cr1.5Mo	0.1	0.2	1.0	0.1	1.5	3.0	0.1
3.5NiCrMoV	0.24	0.01	0.20	3.50	0.45	1.70	0.10
9Cr1Mo	0.10	0.60	0.40	–	1.00	9.00	–
Mod. 9Cr1Mo	0.1	0.35	0.40	0.05	0.95	8.75	0.22
					Nb=0.08	N=0.05	Al <0.04
9Cr$\frac{1}{2}$MoWV	0.11	0.04	0.45	0.05	0.50	9.00	0.20
					W=1.84	Nb=0.07	N=0.05
12CrMoV	0.20	0.25	0.50	0.50	1.00	11.25	0.30
12CrMoVW	0.20	0.25	0.50	0.50	1.00	11.25	0.30
							W=0.35
12CrMoVNb	0.15	0.20	0.80	0.75	0.55	11.50	0.28
						Nb 0.30	N 0.06

Table 2: Typical compositions (wt.%) of creep–resistant steels.

The results of equilibrium calculations which give the phase fractions of the carbides as a function of the overall alloy composition and temperature, are given in Table 3 for the common power plant steels. The calculations have been done using the *MTDATA* [1] computer program and *SGTE* database, taking into account the carbide phases and Laves phase listed, together with cementite. The chemical elements considered are carbon, silicon, manganese, chromium, nickel, molybdenum, vanadium, niobium and nitrogen. M_5C_2 has recently been identified in 1Cr–0.5Mo steels [2] but along with graphite, has not been included in the analysis.

The equilibrium calculations presented in Table 3 are useful in specifying the ultimate microstructure but the results are far removed from the metastable microstructures that exist during service. It is in fact necessary to be able to calculate time–temperature–transformation diagrams for tempering reactions, as a function of steel chemical composition and tempering temperature. In order to do this, a theory capable of handling several simultaneous precipitation reactions has been developed [3,4], where the different phases influence each other, for example by drawing the same solute from the matrix ferrite.

Designation	M_2X	M_7C_3	$M_{23}C_6$	M_6C	Laves	NbC	NbN	VN
$\frac{1}{4}$CrMoV	0.53		2.47					
1CrMoV	0.89		4.12					
2$\frac{1}{4}$Cr1Mo			3.35					
Mod. 2$\frac{1}{4}$Cr1Mo			2.11	0.19				
3.0Cr1.5Mo			1.85	0.57				
3.5NiCrMoV	0.09	1.61	2.85					
9Cr1Mo			2.22					
Mod. 9Cr1Mo			2.22				0.09	0.30
9Cr$\frac{1}{2}$MoWV			2.48		1.35		0.08	0.32
12CrMoV			4.43					
12CrMoVW			4.44		0.07			
12CrMoVNb			3.18			0.06	0.29	0.18

Table 3: The mole percentages of precipitate phases in power plant steels which are in equilibrium at 565 °C (838 K). Notice that cementite is not an equilibrium phase in any alloy.

Overall transformation kinetics A model for a single transformation begins with the calculation of the nucleation and growth rates using classical theory, but an estimation of the volume fraction requires impingement between particles to be taken into account. This is generally done using the extended volume concept of Johnson, Mehl, Avrami, and Kolmogorov [5] as illustrated in Fig. 1. Suppose that two particles exist at time t; a small interval δt later, new regions marked a, b, c & d are formed assuming that they are able to grow unrestricted in extended space whether or not the region into which they grow is already transformed. However, only those components of a, b, c & d which lie in previously untransformed matrix can contribute to a change in the real volume of the product phase (identified by the subscript '1') so that :

$$dV_1 = (1 - \frac{V_1}{V})dV_1^e \qquad (1)$$

where it is assumed that the microstructure develops randomly. The superscript e refers to extended volume, V_1 is the volume of phase 1 and V is the total volume. Multiplying the change in extended volume by the probability of finding untransformed regions has the effect of excluding regions such as b, which clearly cannot contribute to the real change in volume of the product. This equation can easily be integrated to obtain the real volume fraction,

$$\frac{V_1}{V} = 1 - \exp\left\{-\frac{V_1^e}{V}\right\} \qquad (2)$$

Nucleation and growth rates can readily be substituted into V_1^e, leading to the familiar Avrami equation.

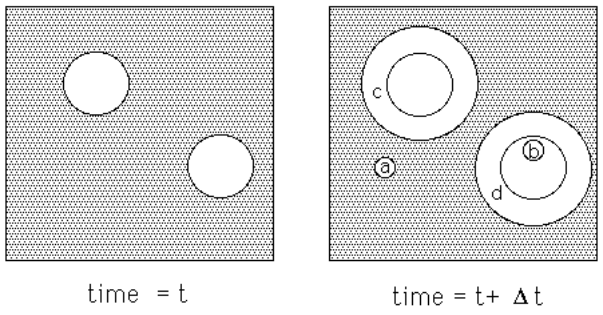

Fig. 1: The concept of extended volume. Two precipitate particles have nucleated and grown to a finite size in the time t. New regions c and d are formed as the original particles grow, but a & b are new particles, of which b has formed in a region which is already transformed.

In practice, there are many cases where several transformations occur together. The different reactions interfere with each other in a way which is seminal to the development of power plant microstructures. The principles involved are first illustrated with an example in which β and θ precipitate at the same time from the parent phase which is designated α. For the sake of discussion it is assumed that the nucleation and growth rates do not change with time and that the particles grow isotropically.

The increase in the extended volume due to particles nucleated in a time interval $t = \tau$ to $t = \tau + d\tau$ is, therefore, given by

$$dV_\beta^e = \frac{4}{3}\pi G_\beta^3 (t-\tau)^3 I_\beta(V)\ d\tau \tag{3}$$

$$dV_\theta^e = \frac{4}{3}\pi G_\theta^3 (t-\tau)^3 I_\theta(V)\ d\tau \tag{4}$$

where G_β, G_θ, I_β and I_θ are the growth and nucleation rates of β and θ respectively, all of which are assumed here to be independent of time. V is the total volume of the system. For each phase, the increase in extended volume will consist of three separate parts. Thus, for β:

(i) β which has formed in untransformed α.

(ii) β which has formed in regions which are already β.

(iii) β which has formed in regions which are already θ.

Only β formed in untransformed α will contribute to the real volume of β. On average a fraction $\left(1 - \frac{V_\beta + V_\theta}{V}\right)$ of the extended volume will be in previously untransformed material. It follows that the increase in real volume of β is given by

$$dV_\beta = \left(1 - \frac{V_\beta + V_\theta}{V}\right) dV_\beta^e \tag{5}$$

and similarly for θ,

$$dV_\theta = \left(1 - \frac{V_\beta + V_\theta}{V}\right) dV_\theta^e \tag{6}$$

Generally V_β will be some complicated function of V_θ and it is not possible to integrate these expressions analytically to find the relationship between the real and extended volumes. Numerical integration is straightforward and offers the opportunity to change the boundary conditions for nucleation and growth as transformation proceeds, to account for the change in the matrix composition during the course of reaction. The method can in principle be applied to any number of simultaneous reactions.

Complex reactions The multiple reactions found in power plant steels have important complications which can all be dealt with in the scheme of simultaneous transformations as presented above. The phases interfere with each other not only by reducing the volume available for transformation, but also by removing solute from the matrix and thereby changing its composition. This change in matrix composition affects the growth and nucleation rates of the phases. The main features of the application of the theory to power plant steels are summarised below; a full description is given in references [3,4].

- The model allows for the simultaneous precipitation of M_2X, $M_{23}C_6$, M_7C_3, M_6C and Laves phase. M_3C is assumed to nucleate instantaneously with the paraequilibrium composition [6]. Subsequent enrichment of M_3C as it approaches its equilibrium composition is accounted for.
- All the phases, except M_3C, form close to their equilibrium composition. The driving forces and compositions of the precipitating phases are calculated using MTDATA [1].
- The interaction between the precipitating phases is accounted for by considering the

change in the average solute level in the matrix as each phase forms.

- The model does not require prior knowledge of the precipitation sequence.
- Dissolution of non–equilibrium phases is incorporated as a natural event.
- A single set of fitting parameters for the nucleation equations (site densities and surface energies) has been found which is applicable to a wide range of power plant steels.

The compositions of three power plant alloys used here for illustration purposes, are shown in Table 4. These three alloys, whilst of quite different chemical compositions, show similar precipitation *sequences* [3,7,8] but with vastly different rates. For example, at 600 °C the time taken before $M_{23}C_6$ is observed is 1 h in the 10CrMoV steel [3], 10 h in the 3Cr1.5Mo alloy [7] and in excess of 1000 h in the $2\frac{1}{4}$Cr1Mo steel [8]. These differences have never before been explained [3,4].

	C	N	Mn	Cr	Mo	Ni	V	Nb
$2\frac{1}{4}$Cr1Mo	0.15	–	0.50	2.12	0.9	0.17	–	–
3Cr1.5Mo	0.1	–	1.0	3.0	1.5	0.1	0.1	–
10CrMoV	0.11	0.056	0.50	10.22	1.42	0.55	0.20	0.50

Table 4: Concentration (in weight%) of the major alloying elements in the steels used to demonstrate the model.

Microstructure Calculations

A plot showing the predicted variation of volume fraction of each precipitate as a function of time at 600 °C is shown in Fig. 2. Consistent with experiments, the precipitation kinetics of $M_{23}C_6$ are predicted to be much slower in the $2\frac{1}{4}$Cr1Mo steel compared to the 10CrMoV and 3Cr1.5Mo alloys. One contributing factor is that in the $2\frac{1}{4}$Cr1Mo steel a relatively large volume fraction of M_2X and M_7C_3 form prior to $M_{23}C_6$. These deplete the matrix and therefore suppress $M_{23}C_6$ precipitation. The volume fraction of M_2X which forms in the 10CrMoV steel is relatively small, and there remains a considerable excess of solute in the matrix, allowing $M_{23}C_6$ to precipitate rapidly. Similarly, in the 3Cr1.5Mo steel the volume fractions of M_2X and M_7C_3 are insufficient to suppress $M_{23}C_6$ precipitation to the same extent as in the $2\frac{1}{4}$Cr1Mo steel.

$M_{23}C_6$ is frequently observed in the form of coarse particles which are less effective in hindering creep deformation. Delaying its precipitation would have the effect of stabilising the finer dispersions of M_2X and MX to longer times with a possible enhancement of creep strength.

Calculations like these can be used to design microstructures exploiting knowledge built up over decades concerning what is good and bad for creep strength. It is often argued that Laves phase formation is bad for creep resistance – it leads to a reduction in the concentration of solid solution strengthening elements; since the Laves precipitates are few and coarse, they do not themselves contribute significantly to strength. The model presented here can be used to design against Laves phase formation. This will be illustrated in later examples.

We note for the moment, that this is as far as microstructure modelling has progressed. The models are not yet capable of giving size distributions and even if that were to be possible, there are no physical models of creep deformation which have sufficient precision to make use of this information. We shall not be discouraged by this since good empirical methods are available. The work described below originates from work by Brun *et al.* [9] and Cole and Bhadeshia [10].

Creep Rupture Strength – the Variables

The basic principles of alloy design for creep resistance are well–established and well–founded on experience. The steels must have a stable microstructure which contains fine alloy carbides to resist the motion of dislocations; however, changes are inevitable over the long service time so that there must be sufficient solid solution strengthening to ensure long term creep resistance. There may be other requirements such as weldability, corrosion and oxidation resistance. It is nevertheless difficult to express the design process quantitatively given the large number of interacting variables.

These variables are described later in the context of calculations in Table 5. For the moment we note that the entire information about microstructure and properties is in principle locked up in this set of parameters since chemical composition and heat treatment are comprehensively included. There may, of course, be many other independent variables that might be considered important in creep analysis, but these are for the moment neglected for two reasons. Firstly, an empirical analysis requires experimental data; an over ambitious list would simply reduce the dataset since publications frequently do not report all of the necessary parameters. Secondly, the effect of any missing variables would simply be reflected in the uncertainties of prediction. If the predictions are noisy then they can be improved with carefully designed exper-

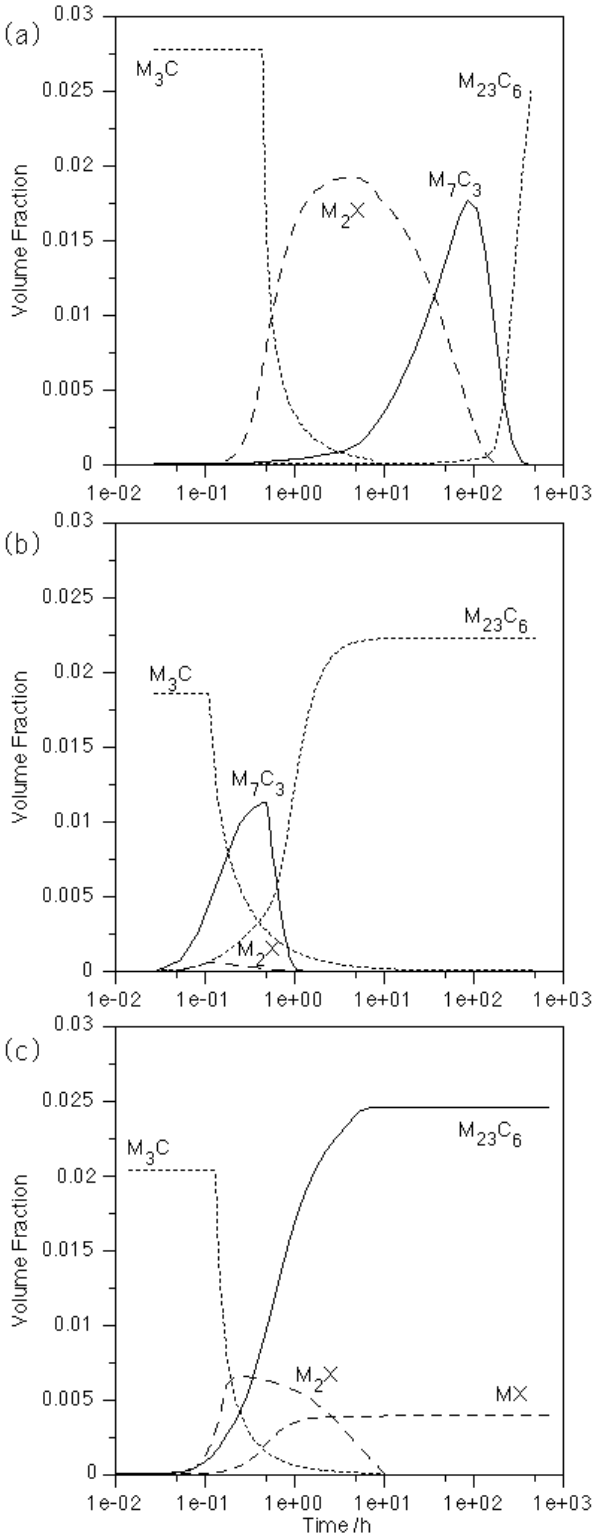

Fig. 2: The predicted evolution of precipitate volume fractions at 600 °C for three power plant materials (a) $2\frac{1}{4}$Cr1Mo (b) 3Cr1.5Mo and (c) 10CrMoV.

iments at a future date. Bearing this in mind, the results to be presented are based on some 2000 sets of experiments obtained from the published literature. We now proceed to describe briefly the methodology.

The Neural Network Method

Most people are familiar with regression analysis where data are best–fitted to a specified relationship which is usually linear. The result is an equation in which each of the inputs x_j is multiplied by a weight w_j; the sum of all such products and a constant θ then gives an estimate of the output $y = \sum_j w_j x_j + \theta$. It is well understood that there are dangers in using such relationships beyond the range of fitted data.

A more general method of regression is neural network analysis. As before, the input data x_j are multiplied by weights, but the sum of all these products forms the argument of a hyperbolic tangent. The output y is therefore a non–linear function of x_j, the function usually chosen being the hyperbolic tangent because of its flexibility. The exact shape of the hyperbolic tangent can be varied by altering the weights (Fig. 3a). Further degrees of non–linearity can be introduced by combining several of these hyperbolic tangents (Fig. 3b), so that the neural network method is able to capture almost arbitrarily non–linear relationships. For example, it is well known that the effect of chromium on the microstructure of steels is quite different at large concentrations than in dilute alloys. Ordinary regression analysis cannot cope with such changes in the form of relationships.

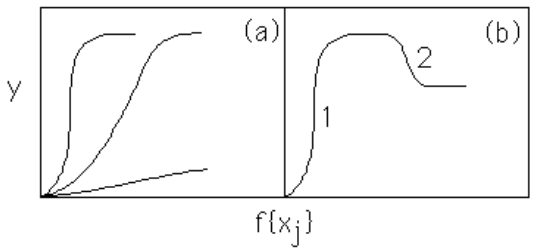

Fig. 3: (a) Three different hyperbolic tangent functions; the "strength" of each depends on the weights. (b) A combination of two hyperbolic tangents to produce a more complex model.

A potential difficulty with the use of powerful regression methods is the possibility of overfitting data (Fig. 4). For example, one can produce a neural network model for a completely random set of data. To avoid this difficulty, the experimental data can be divided into two sets, a *training* dataset and a *test*

dataset. The model is produced using only the training data. The test data are then used to check that the model behaves itself when presented with previously unseen data.

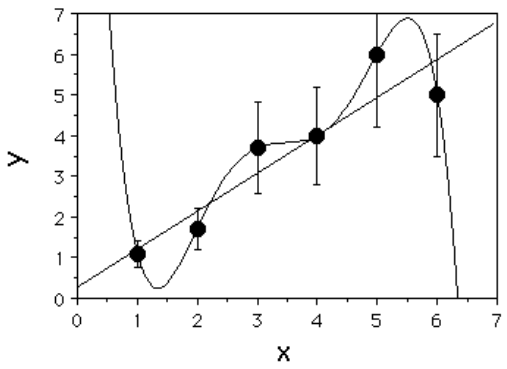

Fig. 4: A complicated model may overfit the data. In this case, a linear relationship is all that is justified by the noise in the data.

Neural network models in many ways mimic human experience and are capable of learning or being trained to recognize the correct science rather than nonsensical trends. Unlike human experience, these models can be transferred readily between generations and steadily developed to make design tools of lasting value. These models also impose a discipline on the digital storage of valuable experimental data, which may otherwise be lost with the passage of time.

The technique is extremely powerful and useful. Its application to creep rupture strength analysis is presented below. The details can be found elsewhere [11] but it is important to note that the generalisation of the model on unseen data has been tested extensively against large quantities of information.

Calculations of Creep Rupture Strength

Fig. 5 shows the variation in the creep rupture strength (10^5 h) of a modern "10CrMoW" creep resistant steel (Table 5) as a function of the temperature, carbon, chromium and molybdenum concentrations. The error bounds represent the uncertainty in fitting the non–linear function to the training data, as 65% confidence limits. There is an additional error associated with each calculation, which is the noise in the experimental data, which is perceived to be of the order of ±2%. The engineering design of power plant is based on the ability to support a stress of 100 MPa for 10^5 h at the service temperature. The apparent insensitivity of the creep rupture strength to the molybdenum or chromium concentrations for 10^5 h is not surprising given that the carbides will all be extremely coarse at that stage of life.

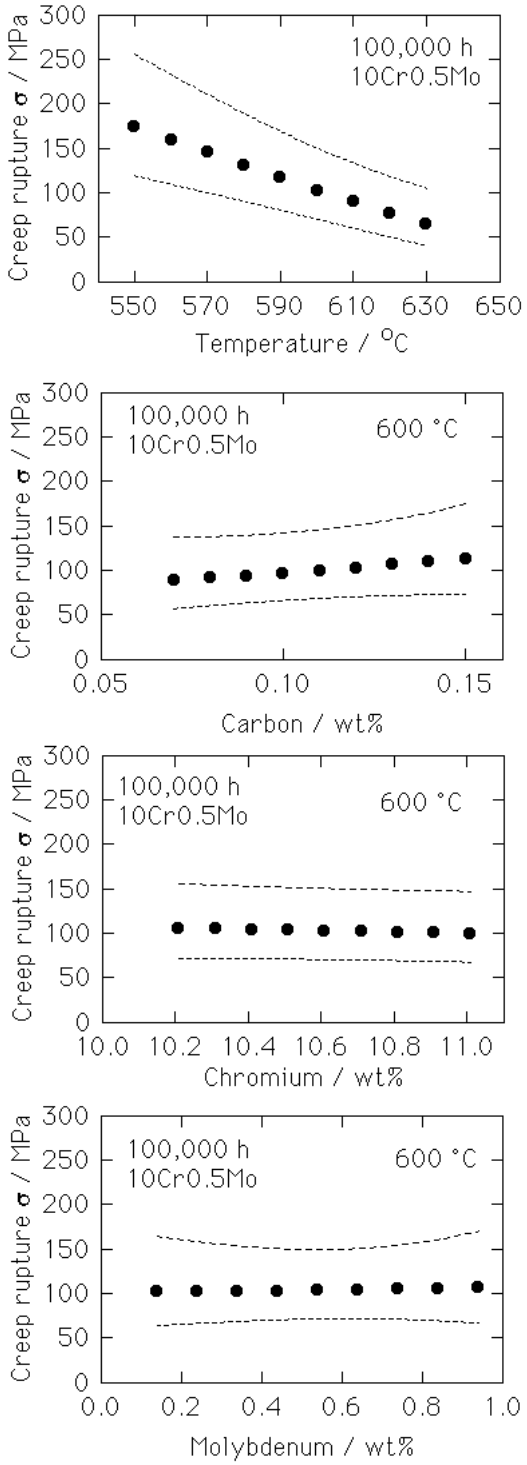

Fig. 5: Creep rupture stress at 600 °C and 100,000 h for 10Cr–0.5Mo type steel

STEEL	$2\frac{1}{4}$CrMo	10CrMoW
Normalising temperature / K	1203	1338
Duration / h	6	2
Cooling rate	water quenched	air cooled
Tempering temperature / K	908	1043
Duration / h	6	4
Cooling rate	air cooled	air cooled
Annealing temperature / K	873	1013
Duration / h	2	4
Cooling rate	air cooled	air cooled
C wt%	0.15	0.12
Si	0.21	0.05
Mn	0.53	0.64
P	0.012	0.016
S	0.012	0.001
Cr	2.4	10.61
Mo	1.01	0.44
W	0.01	1.87
Ni	0.14	0.32
Cu	0.16	0.86
V	0.01	0.21
Nb	0.005	0.01
N	0.0108	0.064
Al	0.018	0.022
B	0.0003	0.0022
Co	0.05	0.015
Ta	0.0003	0.0003
O	0.01	0.01

Table 5: The standard set of input parameters for two alloys used to examine trends predicted by the neural network. The chemical compositions are all in wt.%

Similar data for the classical $2\frac{1}{4}$Cr1Mo steel are illustrated in Fig. 6. The fitting uncertainties are smaller in this case because of the larger quantity of available data since this alloy has been available and studied for a much longer time.

Calculations like these can now be routinely carried out. Furthermore, the models can be improved both as more data become available and as creep deformation becomes better understood. The model can be used in a variety of ways. The combined application of the physical models presented earlier, and the neural network model has led to predictions (see appendix) of novel alloys which ought to have much better creep resistance than any comparable commercial alloy [9]. Another way is to apply the models to welding alloys, for which there are much fewer data when compared with wrought steels.

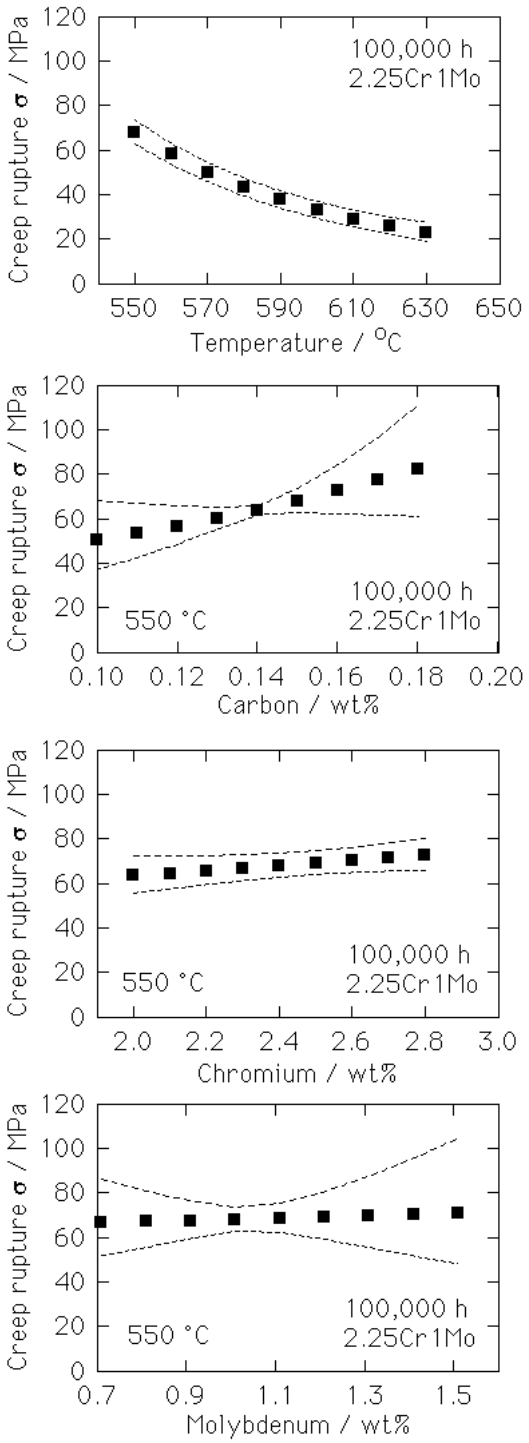

Fig. 6: Creep rupture stress at 600 °C and 100,000 h for 2.25Cr–1Mo type steel

Welding Alloys

Weld metals and steels of matching composition seem to have similar creep rupture properties. In fact, the chemical compositions of weld metals and corresponding steel plates are not very different (Table 6). Of course, weld metal will have a higher oxygen and nitrogen concentration but the former should not affect creep resistance. Although differences in the nitrogen concentration are important, they can easily be taken into account both in predicting carbonitride formation and in the neural network model where nitrogen is an input.

The microstructure of an as–deposited weld metal is naturally radically different from that of a wrought steel. However, even this is unimportant because of the severe tempering heat treatments used following the welding procedure, essentially wipe out the original microstructure and replace it with one which is tempered and similar to that of the steel plate. It is probably for this reason that the welding process itself is found not to influence the creep rupture life [12].

	2.25Cr1Mo		9Cr1Mo	
wt.%	Plate	Weld	Plate	Weld
C	0.110	0.091	0.110	0.090
Mn	0.390	0.590	0.040	0.480
Si	0.290	0.300	0.460	0.500
Cu	0.150	0.024		
Ni	0.150	0.033	0.050	0.050
Cr	2.070	2.480	8.960	8.700
Mo	0.900	1.170	0.470	0.980
Nb			0.069	0.040
V	0.004	0.015	0.200	0.200
S	0.022	0.014		
P	0.011	0.010		
N	0.005	0.010	0.051	0.040
O	0.005	0.030	0.005	0.030

Table 6: Chemical compositions, wt%.

The hypothesis can be proved by examining the data on all–weld metal tests in the published literature [12], again for a stress rupture life of 10^5 h. Such data are most reliable for the $2\frac{1}{4}$Cr1Mo type weld metals; the calculations are therefore presented for the $2\frac{1}{4}$Cr1Mo weld metal listed in Table 6.

Fig. 7 shows the very encouraging agreement between the calculated [9,10] and measured [12] creep rupture lives of $2\frac{1}{4}$Cr1Mo welds. The predictions are made without any adjustment of the models, which did not interrogate any weld metal data during their creation. The results confirm that it is reasonable to assume that weld metal creep rupture life can be modelled on the basis of wrought steels. Of course, other properties such as creep ductility may be more sensitive to inclusion content in which case the weld metals should exhibit a lower ductility relative to the wrought steel.

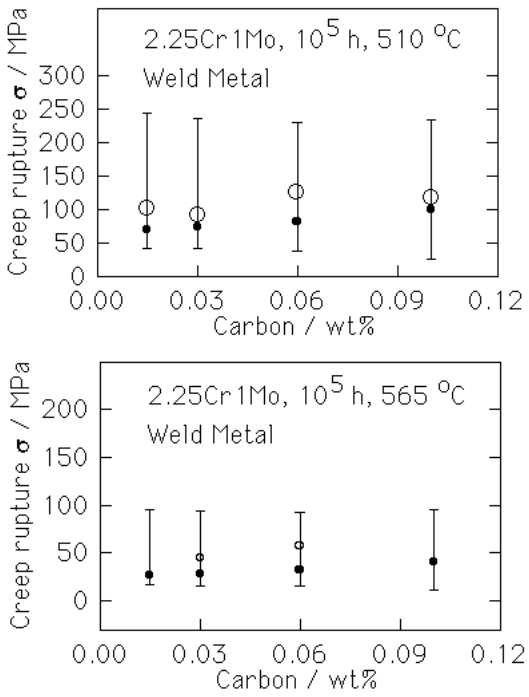

Fig. 7: Calculated (filled circles with error bars) and measured (open circles) stress rupture data for 2.25Cr1Mo weld metal.

The method can now be used to generate creep–rupture diagrams such as that illustrated in Fig. 8.

Conclusions

It is now possible to attempt a quantitative design of heat resistant steels and welding alloys. This is true both with respect to the kinetics of microstructural evolution and in the estimation of creep rupture strength. The combined models provide for the first time an ability to predict new alloys. It would now be interesting for industry to set some challenges, which would stimulate theoretical predictions and finally experimental verification. The whole process from the conception of an alloy to its verification should take much less time than has previously been the case.

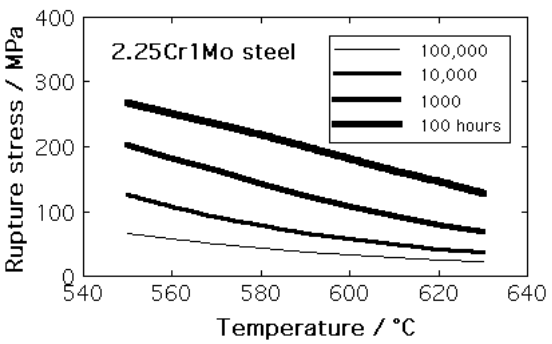

Fig. 8: Calculated stress rupture data for 2.25Cr1Mo weld metal.

In the longer term it is necessary for the microstructure models to predict particle size and spatial distributions, and the effect of stress and strain on transformation kinetics. Such information can then be an input to a more sophisticated mechanical model, perhaps based on dislocation and recovery theory.

Acknowledgments

I am grateful to the organisers of this conference for inviting this lecture, to David Cole and Joe Robson for help with the neural network and microstructural calculations respectively. My sincere thanks also to David MacKay for liberating me from the confines of microstructure calculations; without his ingenious neural network theory I would not have dared to deal with complex mechanical properties.

Appendix

The work presented here is not strictly relevant to welding alloys but is exciting since it will help validate the alloy design philosophy. Brun *et al.* [9] have used the models described in the main text to predict novel steels (Table 7, Fig. 9). The procedure involved a systematic search of the input space focusing on directions which lead to a maximisation of certainty, *i.e.* minimisation of error. The detailed trends investigated are too voluminous to report here. The calculations involved the modification of the standard 10CrMoW steel (Table 7) so all the results are compared against that alloy. The first attempt led to the design of alloy A (Table 7) but its long term properties at 650 °C just fail to meet the 100 MPa requirement (Fig. 9). Changes were therefore made to improve both the mean long term properties and the certainty in their prediction, by reducing the cobalt, chromium and molybdenum concentrations.

The new alloys do not contain any silicon, aluminium, nickel or copper, all of which can be demonstrated to lead to a deterioration in the creep rupture stress. The boron concentration is kept small primarily to reduce the uncertainty in the predictions. There is an increase in the normalizing temperature, and reductions in the manganese and chromium concentrations together with an increase in the level of tungsten. The kinetics of carbide precipitation, phase stability calculations and the kinetics of intermetallic Laves phase precipitation have all been carried out for these novel steels. These calculations indicate a "desirable" sequence of precipitation, the absence of detrimental phases and a large temperature range over which the steels are fully austenitic (*i.e.* can be processed hot). The steels have been manufactured by Nippon Steel but at present are undergoing creep tests (which inevitably take time) so there is nothing more to report until the next conference in this series!

References

1. MTDATA: *Metallurgical Thermochemistry Group,* National Physical Laboratory, Teddington, London (1998)
2. S. D. Mann, D. G. McCulloch and B. C. Muddle: *Metallurgical and Materials Transactions A* 26A, 509–520(1995)
3. J. D. Robson and H. K. D. H. Bhadeshia: *Mat. Sci. Tech.* 13, 631–644(1997)
4. J. D. Robson and H. K. D. H. Bhadeshia: *Calphad* 20 447–460(1996)
5. J. W. Christian: *Theory of Transformations in Metals and Alloys,* Pergamon Press, Oxford, 2nd edition, part I (1975)
6. H. K. D. H. Bhadeshia: *Materials Science and Technology* 5, 131–137.(1989)
7. N. Fujita and H. K. D. H. Bhadeshia: *Advanced Heat Resistant Steels for Power Generation,* San Sebastian, published by the Institute of Materials, London 223–233.(1998)
8. R. G. Baker and J. Nutting: *Journal of the Iron and Steel Institute* 192, 257–268(1959)
9. F. Brun, T. Yoshida, J. D. Robson, V. Narayan and H. K. D. H. Bhadeshia: *Materials Science and Technology* 15 547–555(1999)
10. D. Cole, C. Martin–Moran, A. Sheard, H. K. D. H. Bhadeshia and D. J. C. MacKay: *Science and Technology of Welding and Joining* 5 81–89(2000)
11. D. J. C. MacKay: *Neural Computation* 4, 415-472(1992)

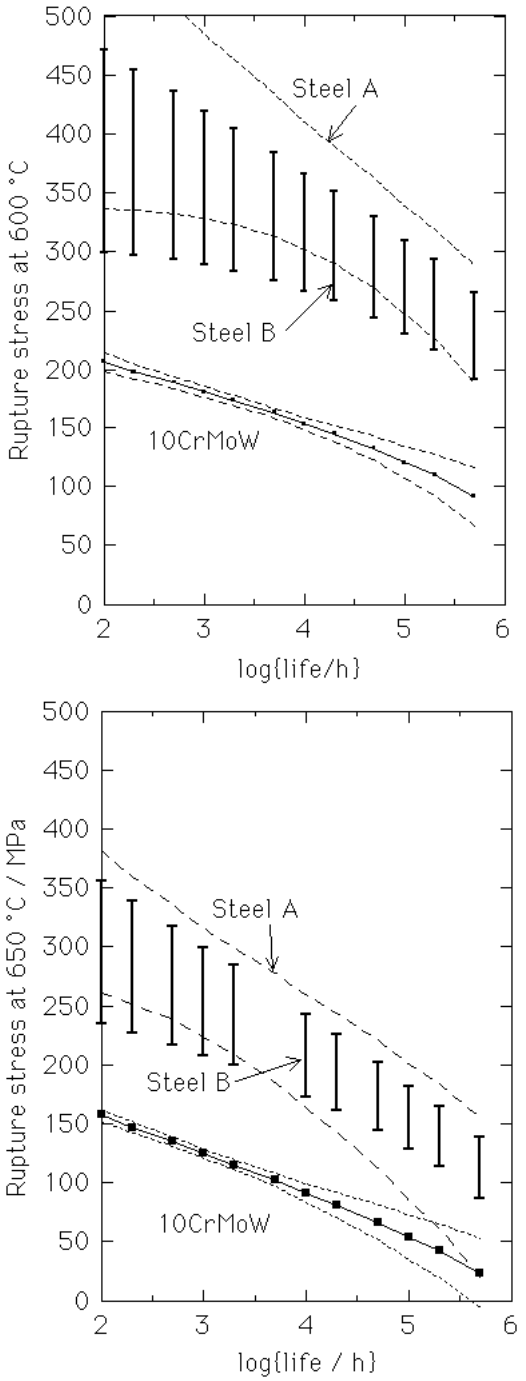

Fig. 9: Calculated stress rupture strength as a function of time for 600 and 650 $°C$ for the standard 10CrMoW steel, steel A and steel B. For clarity, only the error bounds are presented for steels A and B. The mean values lie precisely between the error bounds.

12. C. D. Lundin, S. C. Kelley, R. Menon and B. J. Kruse: *Welding Research Council bulletin 277,* New York 1–66(1986)

STEEL	10CrMoW	A	B
Normalizing temperature / K	1338	1473	1453
Duration / h	2	2	2
Cooling rate	air cooling	air cooling	air cooling
Tempering temperature K	1043	1073	1073
Duration / h	4	4	4
Cooling rate	air cooling	air cooling	air cooling
Annealing temperature / K	1013	1013	1013
Duration / h	4	4	4
Cooling rate	air cooling	air cooling	air cooling
C wt.%	0.12	0.12	0.13
Si	0.05	0	0
Mn	0.64	0.48	0.5
P	0.016	0.0016	0.0016
S	0.001	0.001	0.001
Cr	10.61	9	8.7
Mo	0.44	0.75	0.3
W	1.87	3	3
Ni	0.32	0	0
Cu	0.86	0	0
V	0.21	0.21	0.21
Nb	0.01	0.01	0.01
N	0.064	0.064	0.064
Al	0.022	0	0
B	0.0022	0.008	0.008
Co	0.015	1.25	0
Ta	0.0003	0.0003	0.0003
O	0.01	0.01	0.01
Re	0.0003	0.0003	0.0003

Table 7: The input parameters for the standard 10CrMoW steel and steels A and B.